Figures and figure supplements

Analysis of SMAD1/5 target genes in a sea anemone reveals ZSWIM4-6 as a novel BMP signaling modulator

Paul Knabl and Alexandra Schauer *et al*.

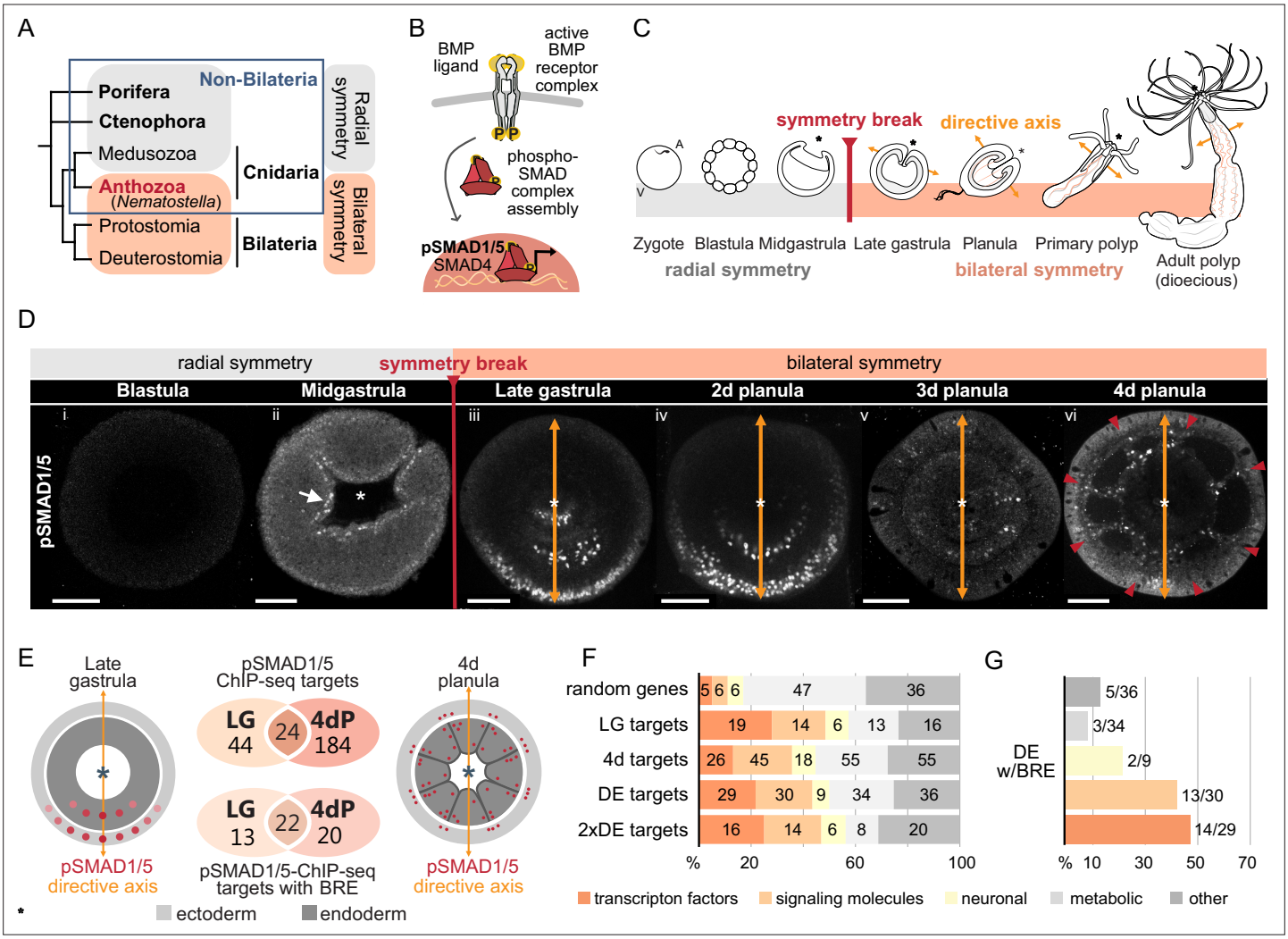

Figure 1. Bilateral body symmetry of the non-bilaterian sea anemone *Nematostella* is BMP signaling-dependent. (**A**) Bilateral body symmetry is observed in Bilateria and in anthozoan Cnidaria. (**B**) BMP signaling is initiated by BMP ligands binding to BMP receptors that trigger phosphorylation, assembly, and nuclear translocation of a pSMAD1/5/SMAD4 complex to regulate gene expression. (**C**) A BMP signaling-dependent symmetry break at late gastrula (LG) stage results in the formation of the secondary (directive) body axis in the sea anemone *Nematostella*. (**D**) BMP signaling dynamics during *Nematostella* development. No pSMAD1/5 is detectable in the blastula (**Di**). Nuclear pSMAD1/5 is localized in the blastopore lip of midgastrula (**Dii**), forms a gradient along the directive axis in the LG (**Diii**) and 2d planula (**Div**). By day 3, the gradient progressively disperses (**Dv**), and the signaling activity shifts to the eight forming endodermal mesenteries (**Dvi**) and to the ectodermal stripes vis-à-vis the mesenteries (arrowheads). Images (**Dii–Dvi**) show oral views (asterisks). Scale bars 50 µm. (**E**) Comparison of the direct BMP signaling targets at LG and 4dP shows little overlap. Schemes show oral views of a LG and a 4dP with red spots indicating the position of pSMAD1/5-positive nuclei in the ectoderm (light gray) and endoderm (dark gray). (**F**) Transcription factors, signaling molecules, and neuronal genes are overrepresented among the pSMAD1/5 targets compared to the functional distribution of 100 random genes. LG, late gastrula targets; 4dP, 4d planula targets; DE, pSMAD1/5 ChIP targets differentially expressed in BMP2/4 and/or GDF5-like morphants ($p_{adj} \leq 0.05$); 2xDE targets, pSMAD1/5 ChIP targets differentially expressed in BMP2/4 and/or GDF5-like morphants ($p_{adj} \leq 0.05$) showing ≥2-fold change in expression. (**G**) Fractions of each functional category of the differentially expressed pSMAD1/5 target genes (see panel **F**) containing BMP response elements (BREs).

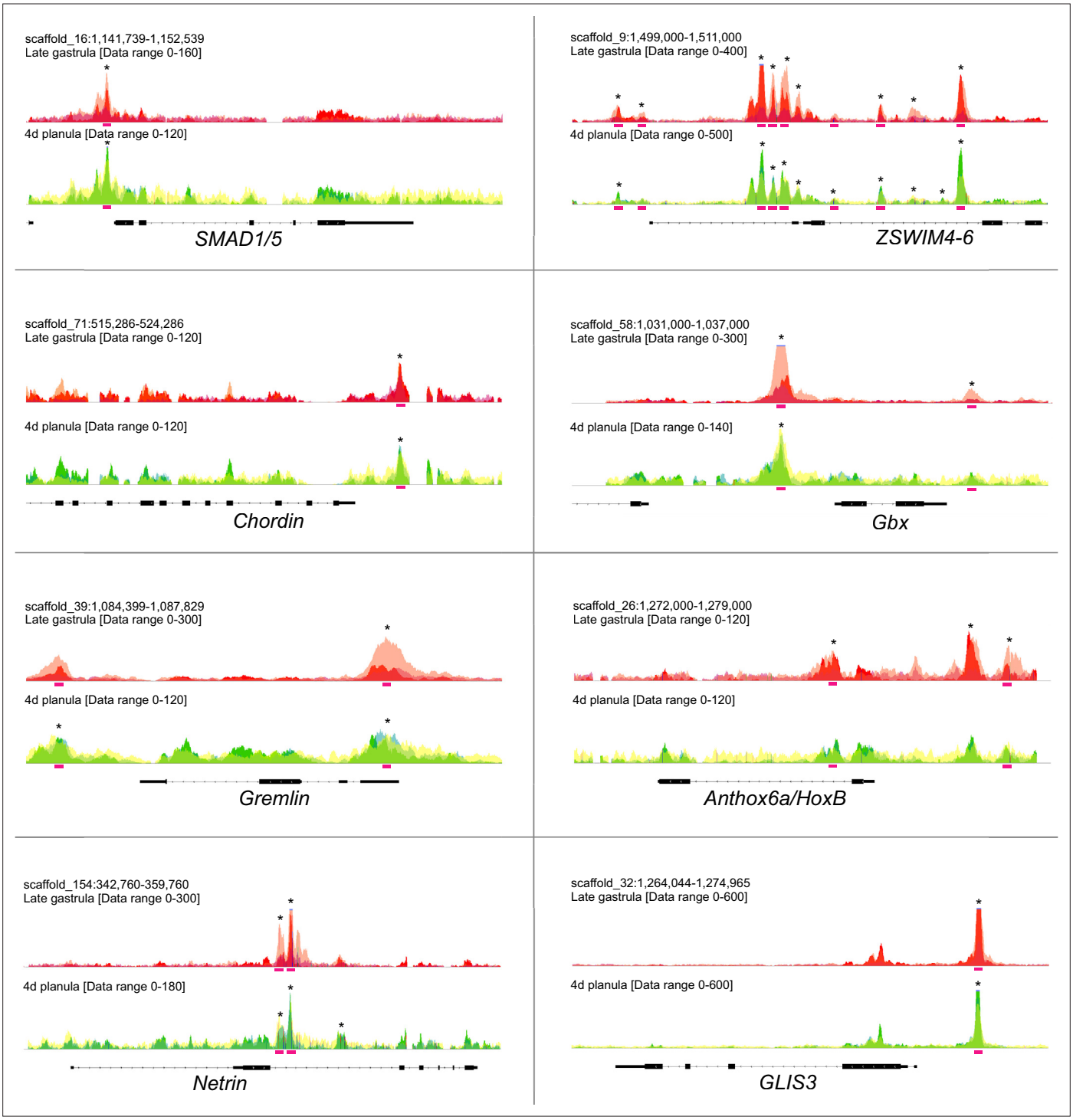

Figure 1—figure supplement 1. Sequencing coverage profile shows the enrichment of pSMAD1/5 binding at the target genes. Overlays of the three biological replicates are shown. Statistically significant peaks are marked with asterisks. Pink bars, BMP response elements (BREs).

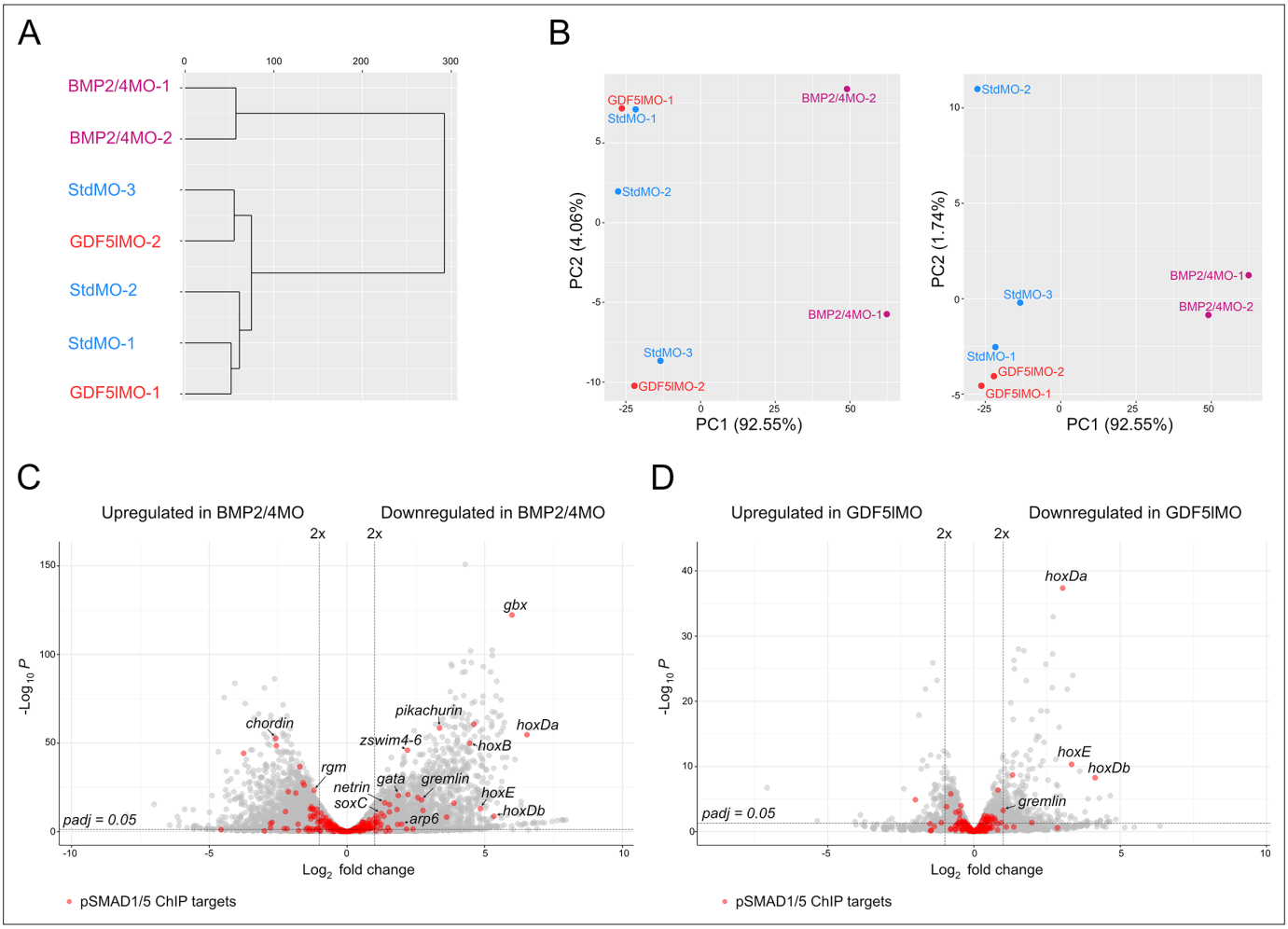

Figure 1—figure supplement 2. Transcriptomic comparison of BMP2/4, GDF5-like, and control morphants and differential expression of pSMAD1/5 ChIP targets upon different knockdowns. (**A**) In the cluster dendrogram and (**B**) principal component analysis, replicates of GDF5lMO (red) and StdMO (blue) transcriptomes group together, while the transcriptome of BMP2/4MO (magenta) is separated. (**C, D**) Volcano plots highlight differentially expressed pSMAD1/5 ChIP targets (red) in (**C**) BMP2/4 morphants and (**D**) GDF5-like morphants ($p_{adj} \leq 0.05$).

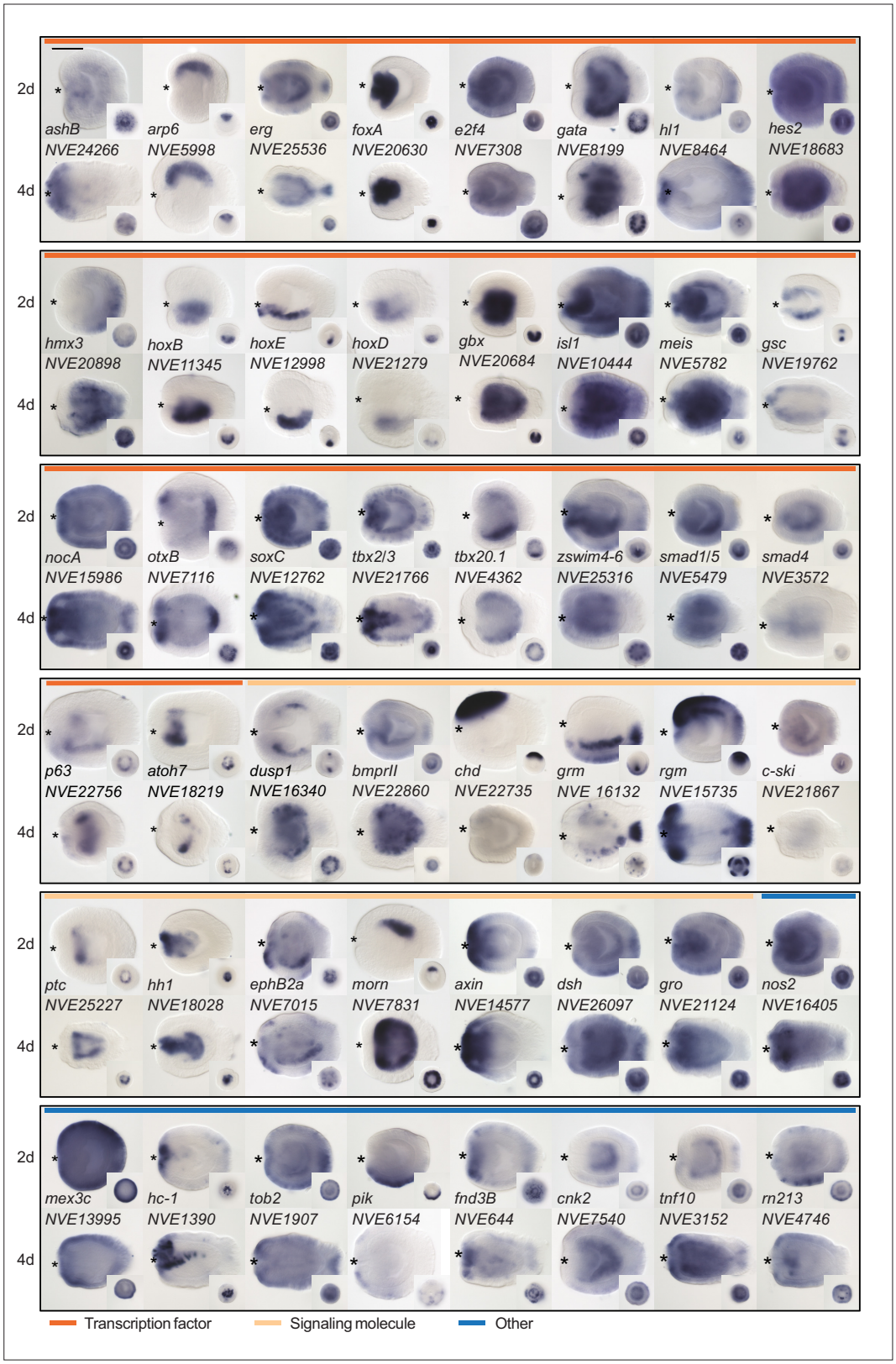

Figure 2. Expression patterns of a selection of the direct targets of BMP signaling in 2d and 4d planulae. In lateral views, the oral end is marked with an asterisk, inlets show oral views. Scale bar 100 µm.

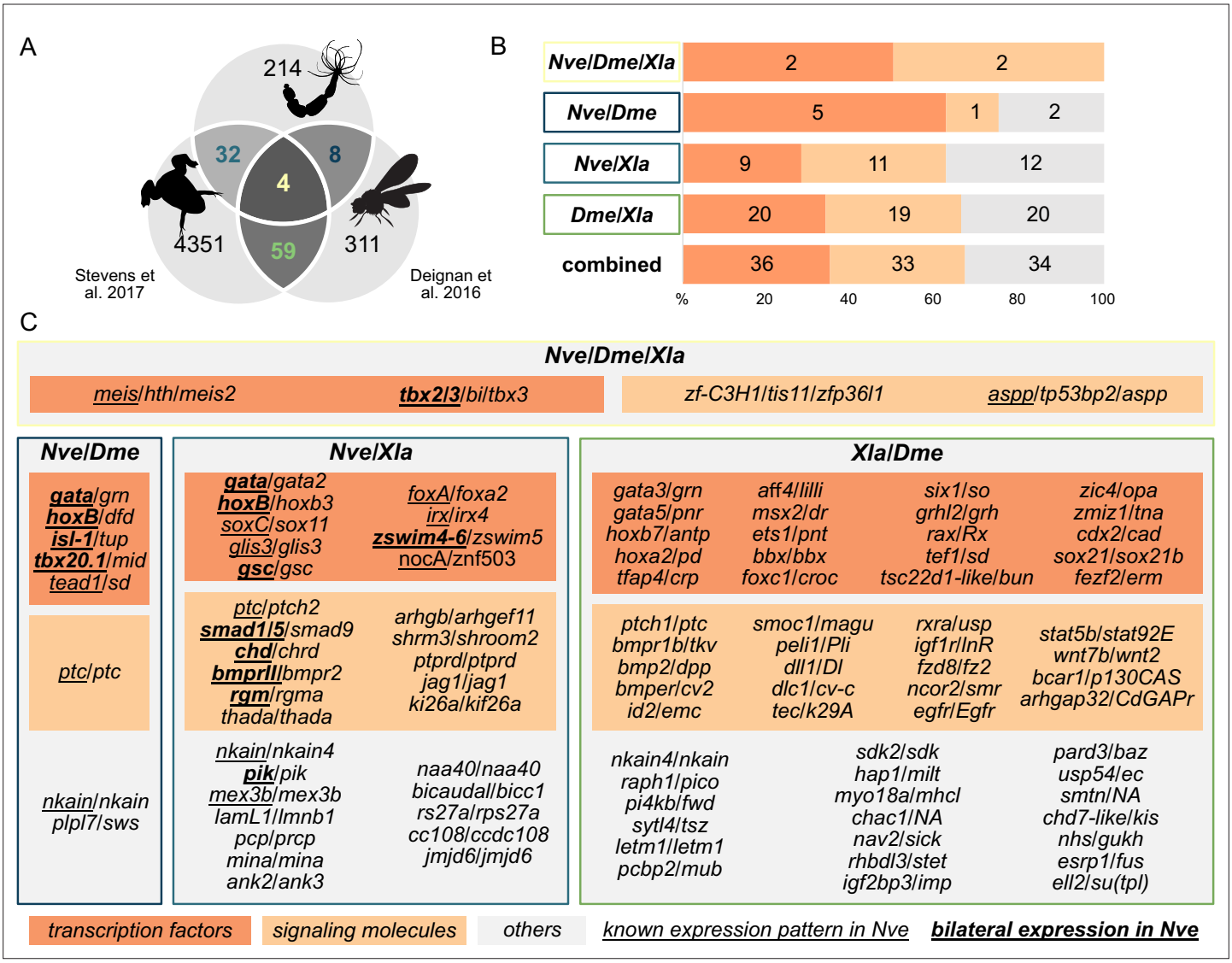

Figure 3. *Nematostella* and Bilateria share BMP signaling targets, which predominantly encode transcription factors and signaling molecules. (**A**) Overlap of BMP signaling targets at comparable embryonic stages in the three-way comparison of *Nematostella*, *Drosophila* (***Deignan et al., 2016***), and *Xenopus* (***Stevens et al., 2017***). Orthology links were deduced by NCBI BLASTP of the respective proteomes with a cut-off e-value ≤ 1e-5, and reciprocal best BLAST hits were determined using the bit score. (**B**) Transcription factors and signaling molecules represent more than 60% of pSMAD1/5 targets shared between *Nematostella* (*Nve*), fly (*Dme*), and frog (*Xla*). (**C**) Gene names of orthologous targets shared between *Nematostella*, fly, and frog. For targets shared with *Nematostella*, genes with known expression patterns in the embryo are underlined, while genes expressed asymmetrically along the directive axis are underlined and bold.

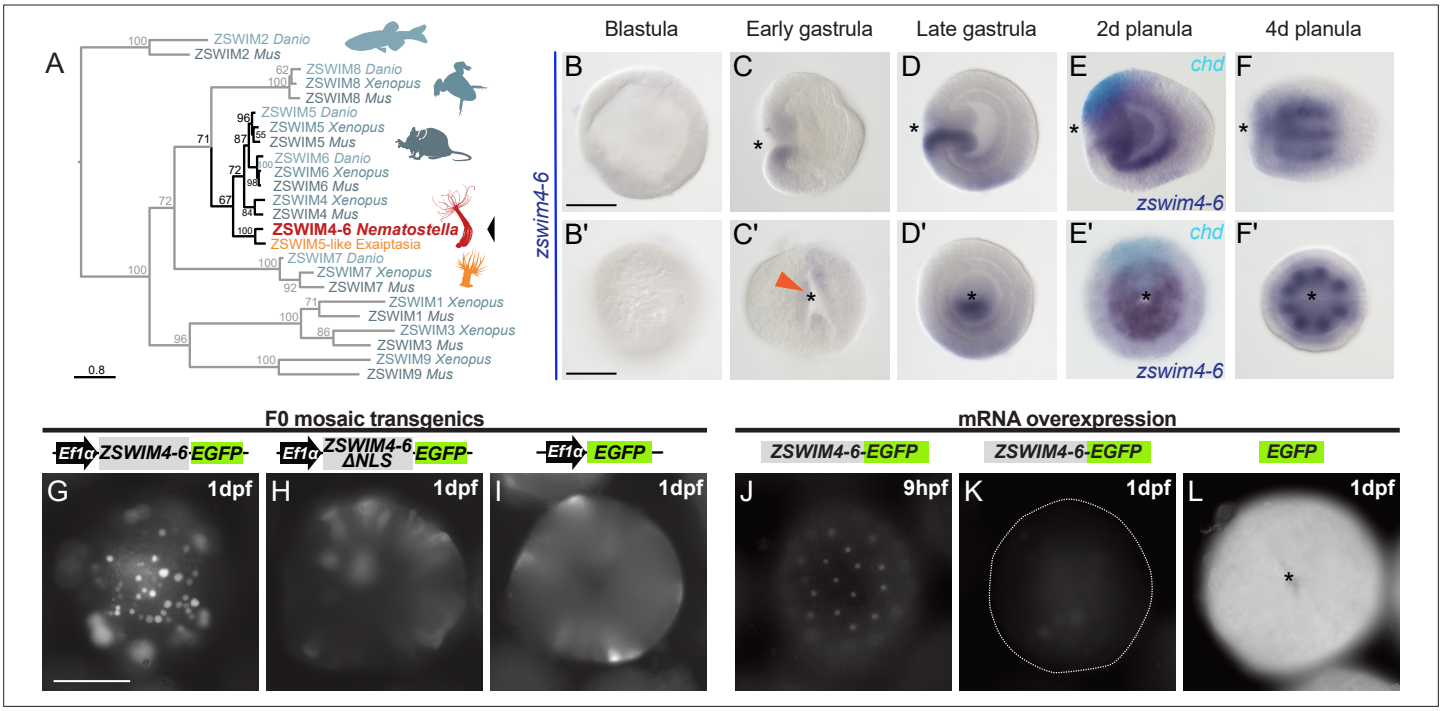

Figure 4. *zswim4-6* is a target of BMP signaling with bilaterally symmetric expression and encodes a nuclear protein. (**A**) Maximum likelihood phylogeny shows that *Nematostella* ZSWIM4-6 clusters with ZSWIM4, ZSWIM5, and ZSWIM6 from zebrafish, frog, and mouse. (**B–F'**) *Nematostella zswim4-6* expression follows the dynamic BMP signaling domain (see ***Figure 1D*** for comparison). Double ISH shows *zswim4-6* and *chd* transcripts localize to the opposite sides of the directive axis. (**G–I**) Mosaic expression of ZSWIM4-6-EGFP under the control of the ubiquitously active *EF1α* promoter in F0 transgenic animals demonstrates that ZSWIM4-6 is a nuclear protein. Full-length ZSWIM4-6-EGFP is translocated into the nuclei (**G**), while ZSWIM4-6ΔNLS-EGFP missing the predicted nuclear localization signal NLS remains cytoplasmic (**H**), similar to the EGFP control (**I**). Exposure time was the same in all images. (**J–L**) Microinjection of *ZSWIM4-6-EGFP* mRNA results in a weak EGFP signal detectable in the nuclei of the early blastula (**J**), which progressively disappears towards late gastrula (**K**). EGFP translated from *EGFP* mRNA remains readily detectable (**L**). To visualize the weak signal in (**J–K**), the exposure had to be increased in comparison to (**L**). Asterisks mark the oral side; scale bars 100 µm.

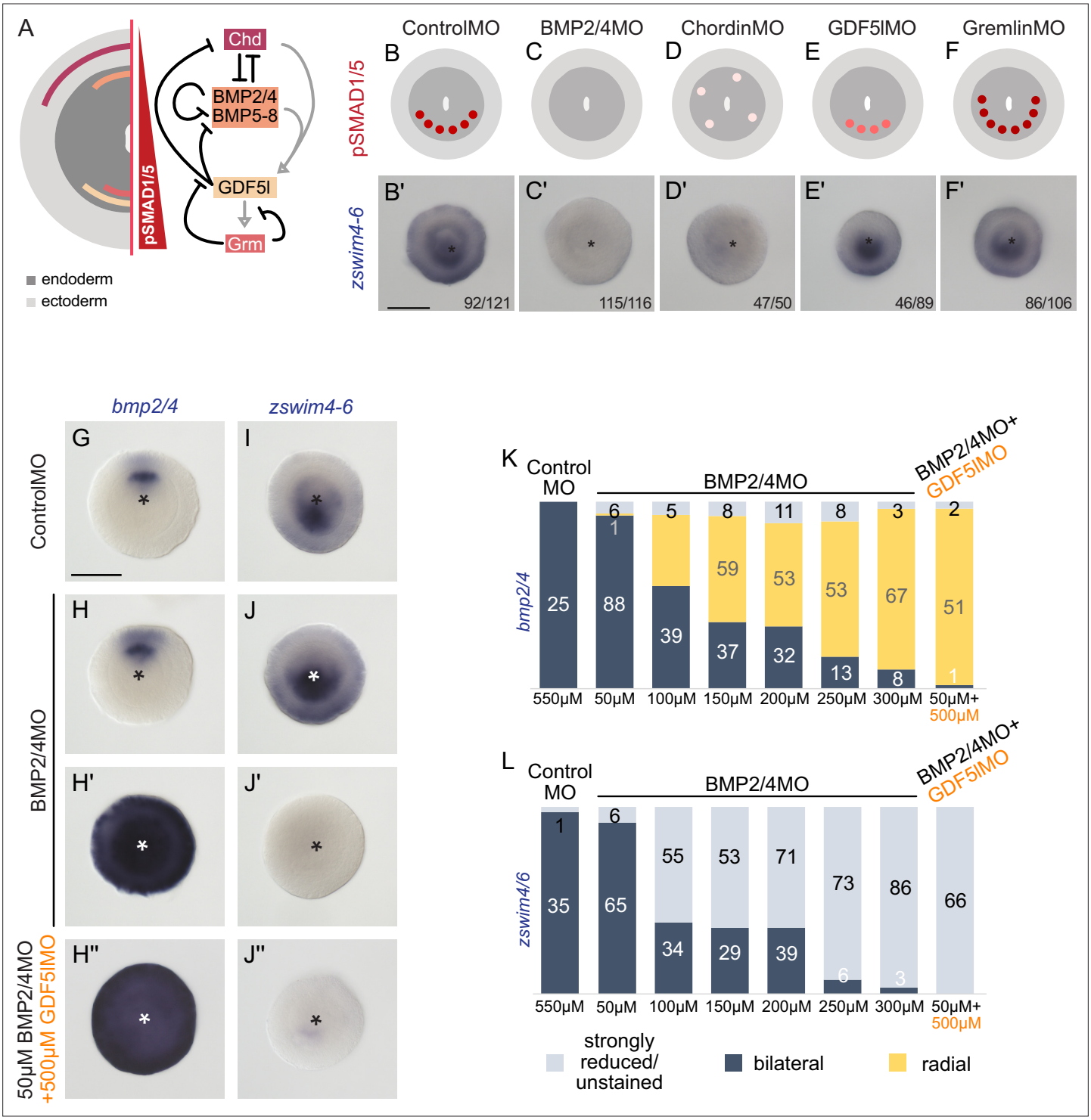

Figure 5. *zswim4-6* reacts differently to the downregulation of BMP2/4 and GDF5-like. (**A**) Expression domains and putative interactions of the BMP network components in 2d embryos (based on ***Genikhovich et al., 2015***). (**B–F'**) Effect of the knockdown (KD) of the individual BMP signaling components on nuclear pSMAD1/5 and on *zswim4-6* expression. *zswim4-6* expression is abolished upon KD of *bmp2/4* and *chordin*, but not in KD of *gdf5-l* and *gremlin*. Sketches in (**B–F**) show that the gradient is lost upon BMP2/4 and Chd KD, reduced upon GDF5-like KD and expanded upon Gremlin KD (based on ***Genikhovich et al., 2015***). (**G–L**) KD of *bmp2/4* using different concentrations of BMP2/4MO results in either normal, bilaterally symmetric marker expression or complete radialization but no intermediate phenotypes. Instead, the penetrance of the radialization phenotype increases with the increase of the BMP2/4MO concentration. Co-injection of the lowest, ineffective BMP2/4MO concentration with GDF5lMO also results in a complete radialization. All stainings are performed on 2d planulae. Scale bars 100 µm.

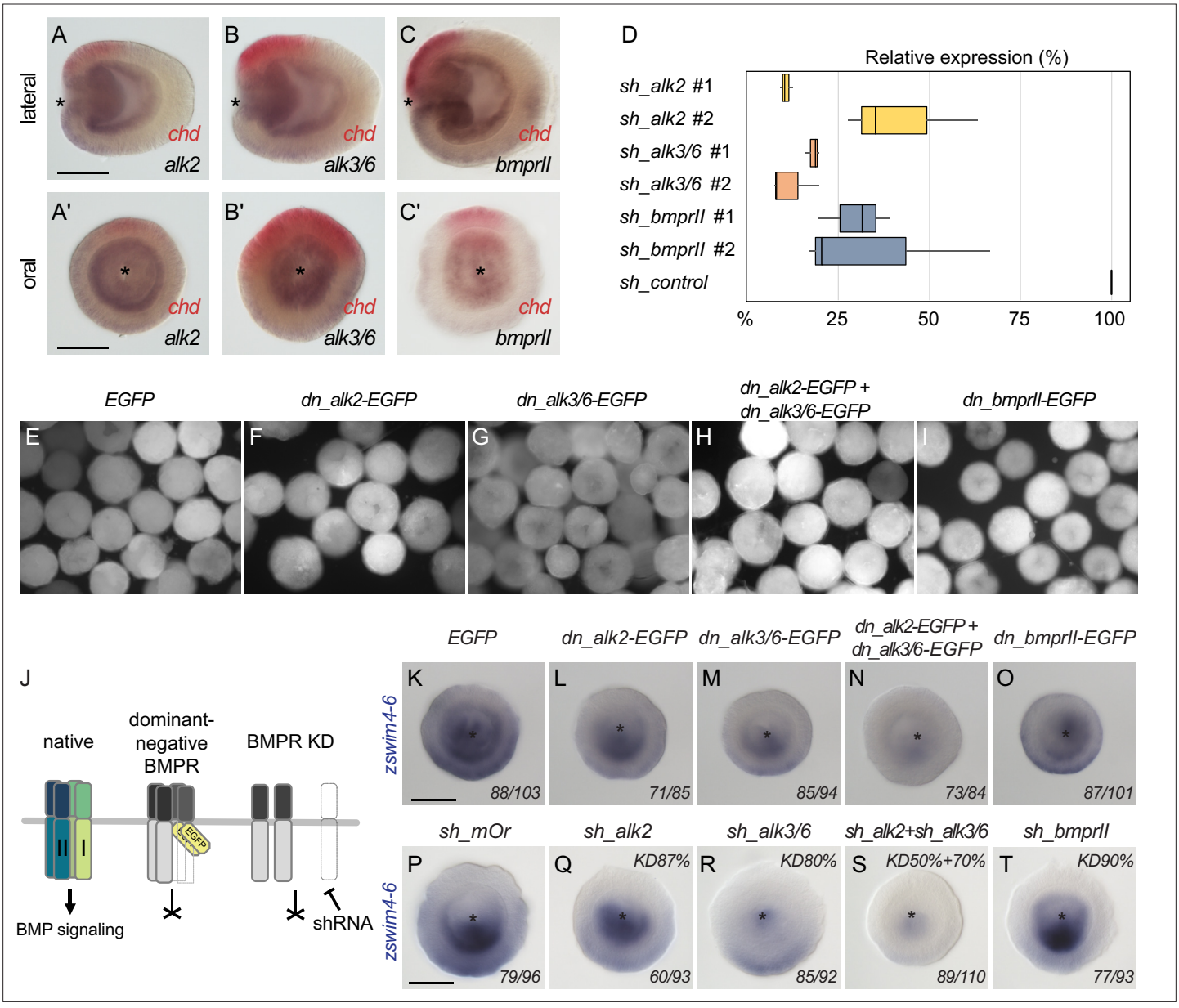

Figure 5—figure supplement 1. Two type I BMP receptors display partial redundancy in regulating *zswim4-6* expression. Expression of BMP receptors (**A, A'**) *alk2,* (**B, B'**) *alk3/6,* and (**C, C'**) *bmprII* is broadly detectable in endoderm with a slightly stronger expression on the 'strong BMP signaling' side of the directive axis, opposite to *chordin* (red). (**D**) qPCR quantification of knockdown (KD) efficiency for BMP receptor shRNAs in relation to shRNA against mOrange (sh_control, 100% expression). Black lines represent the median. (**E–I**) EGFP signal in late gastrula embryos injected with (**E**) *EGFP* mRNA and (**F–I**) mRNA of dominant-negative BMP receptor constructs in which Ser/Thr-kinase domain was replaced with the *EGFP* coding sequence. (**J**) Overview of the expected effect of the dominant negative BMP receptor overexpression and BMP receptor RNAi on BMP signaling. (**K–O**) *zswim4-6* expression is weakly reduced upon overexpression of the dominant negative type I BMP receptors dnAlk2-EGFP and dn_Alk3/6-EGFP and strongly suppressed upon combined overexpression of dn_Alk2-EGFP and dn_Alk3/6-EGFP but remains unchanged upon overexpression of the dominant negative type II BMP receptor dn_BMPRII-EGFP. (**P–T**) Expression of *zswim4-6* is weakly reduced upon Alk2 RNAi, the effect is stronger upon Alk3/6 KD, and *zswim4-6* is practically abolished in a combined Alk2+Alk3/6 KD. zswim4-6 expression is unaffected by the BMPRII RNAi. Asterisks mark the oral side. Scale bars 100 µm. The numbers in the bottom-right corner indicate the ratio of embryos displaying the phenotype shown in the image to the total number of embryos treated and stained as indicated in the figure. In (**P–T**), KD efficiency is shown in the top-right corner of each image.

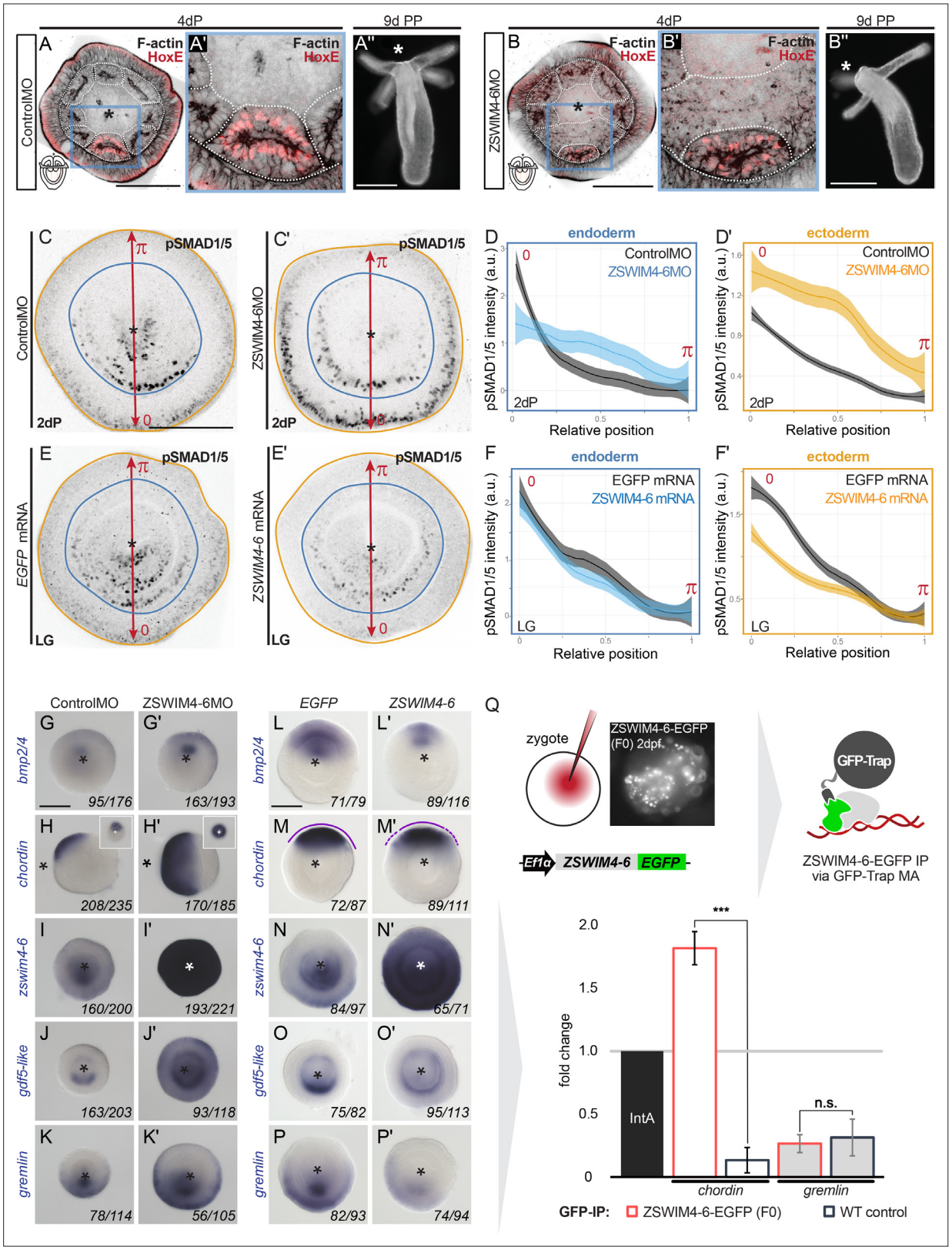

Figure 6. ZSWIM4-6 is a modulator of BMP signaling that appears to act as transcriptional repressor. (**A–B″**) Morpholino knockdown (KD) of *zswim4-6* results in patterning defects. (**A**) and (**B**) show confocal sections across the pharyngeal region of 4d planulae stained with antiHoxE antibody (***Genikhovich et al., 2015***) and phalloidin. (**A′**) and (**B′**) show the areas boxed in (**A**) and (**B**). White dotted lines delineate mesenterial chambers. In the 4d planula, the HoxE-positive mesenterial chamber does not reach the pharynx, which leads to the fusion of neighboring chambers (compare **A**, **A′** with

Figure 6 continued on next page

Figure 6 continued

B, **B'**). This results in the formation of three instead of four tentacles in the 9d polyp (compare **A''** with **B''**). (**C–F'**) Immunofluorescence and quantification of relative nuclear anti-pSMAD1/5 staining intensities in 2d ZSWIM4-6 morphants (**C–D'**) and upon *zswim4-6* mRNA overexpression in the late gastrula (**E–F'**). Intensity measurements (arbitrary units, a.u.) are plotted as a function of the relative position of each nucleus in the endoderm or in the ectoderm along a 180° arc from 0 (high signaling side) to π (low signaling side). The measurements from Control MO embryos (n = 10) and ZSWIM4-6MO embryos (n = 10), as well as *egfp* mRNA embryos (n = 22 for the endodermal, and n = 24 for the ectodermal measurements) and *zswim4-6* mRNA embryos (n = 8 for the endodermal, and n = 9 for the ectodermal measurements) are described by a LOESS smoothed curve (solid line) with a 99% confidence interval for the mean (shade). For visualization purposes, the intensity values were normalized to the upper quantile value among all replicates and conditions of each control-experiment pair. (**G–K'**) Expression of *zswim4-6* and BMP network components in the 2d planula upon morpholino KD of *zswim4-6*; All images except for (**H**) and (**H'**) show oral views. (**L–P'**) Expression of *zswim4-6* and BMP network components in late gastrula (30 hr) upon *zswim4-6* mRNA injection; oral views, purple dashed line marks the loss of a sharp boundary of *chd* expression. In (**A–P'**), asterisks mark the oral side. In (**A-P'**), scale bars 100 µm. (**Q**) ChIP with GFP-Trap detects ZSWIM4-6-EGFP fusion protein in the vicinity of the pSMAD1/5 binding site in the upstream regulatory region of *chordin* but not of *gremlin*. Experiment on biological quadruplicates. Mean enrichments and standard deviations are shown.

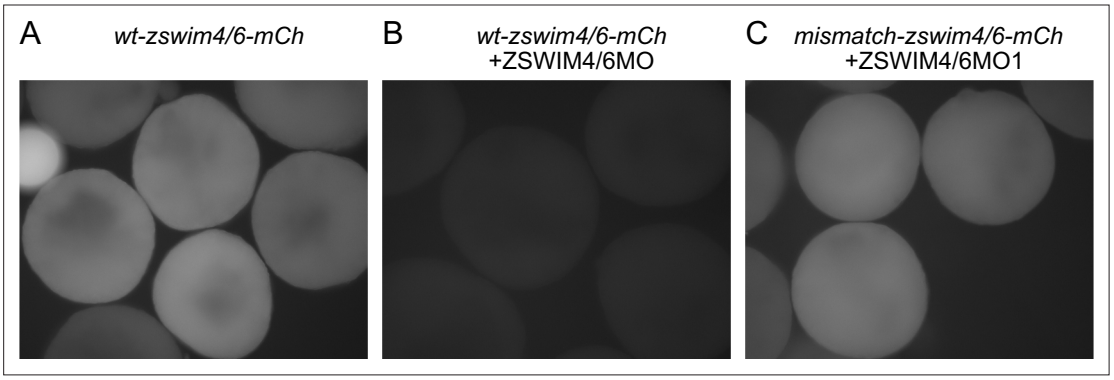

Figure 6—figure supplement 1. Testing ZSWIM4/6 morpholino specificity. (**A**) Fluorescent signal in embryos injected with mRNA coding for the ZSWIM4/6 recognition sequence fused to the mCherry (*wt-zswim4/6-mCh*) coding sequence. (**B**) Co-injection with ZSWIM4/6 morpholino can suppress the translation of mRNAs containing the respective recognition sequence. (**C**) Translation of mRNA coding for the zswim4/6 recognition sequence carrying five mismatches and fused to mCherry (*mismatch-zswim4/6-mCh*) is no longer suppressed when co-injected with ZSWIM4/6 morpholino.

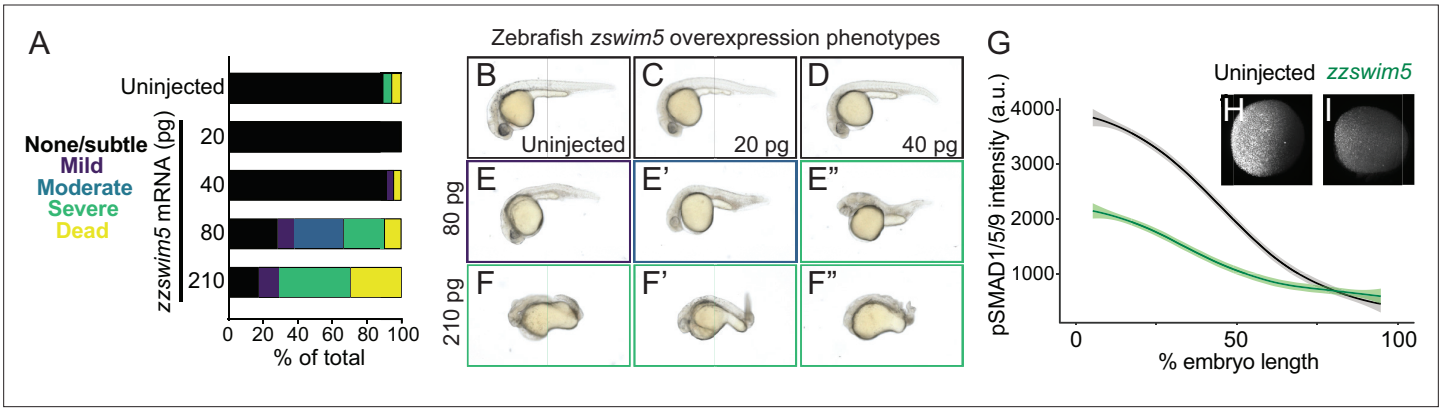

Figure 6—figure supplement 2. *zzswim5* overexpression dampens BMP signaling and causes developmental defects in zebrafish. (**A–F″**) Wild-type zebrafish embryos were left uninjected (**B**) or injected at the one-cell stage with 20, 40, 80, or 210 pg *zzswim5* mRNA. (**A**) Phenotype quantification at 1 d post-fertilization (dpf) shows increasingly severe developmental defects at higher amounts of mRNA. A representative selection was imaged at 1 dpf (**B–F″**). Multiple embryos are shown for 80 (**E–E″**) and 210 (**F–F″**) pg to illustrate the variety of defects. Number of embryos – uninjected: 19, 20 pg: 20, 40 pg: 24, 80 pg: 21, 210 pg: 17. (**G–I**) Embryos were injected with 80 pg *zzswim5* mRNA or left uninjected and fixed at 50% epiboly (early gastrulation). BMP signaling levels were assessed using pSmad1/5/9 immunostaining. Animal pole views are shown with ventral on the left. (**G**) Quantification of immunofluorescence (arbitrary units, a.u.) reveals lower amplitude BMP signaling gradients in *zzswim5*-overexpressing embryos (**I**) compared to uninjected controls (**H**). The measurements from uninjected embryos (n = 8) and *zzswim5*-injected embryos (n = 8) are described by a LOESS smoothed curve (solid line) with a 99% confidence interval for the mean (shade).

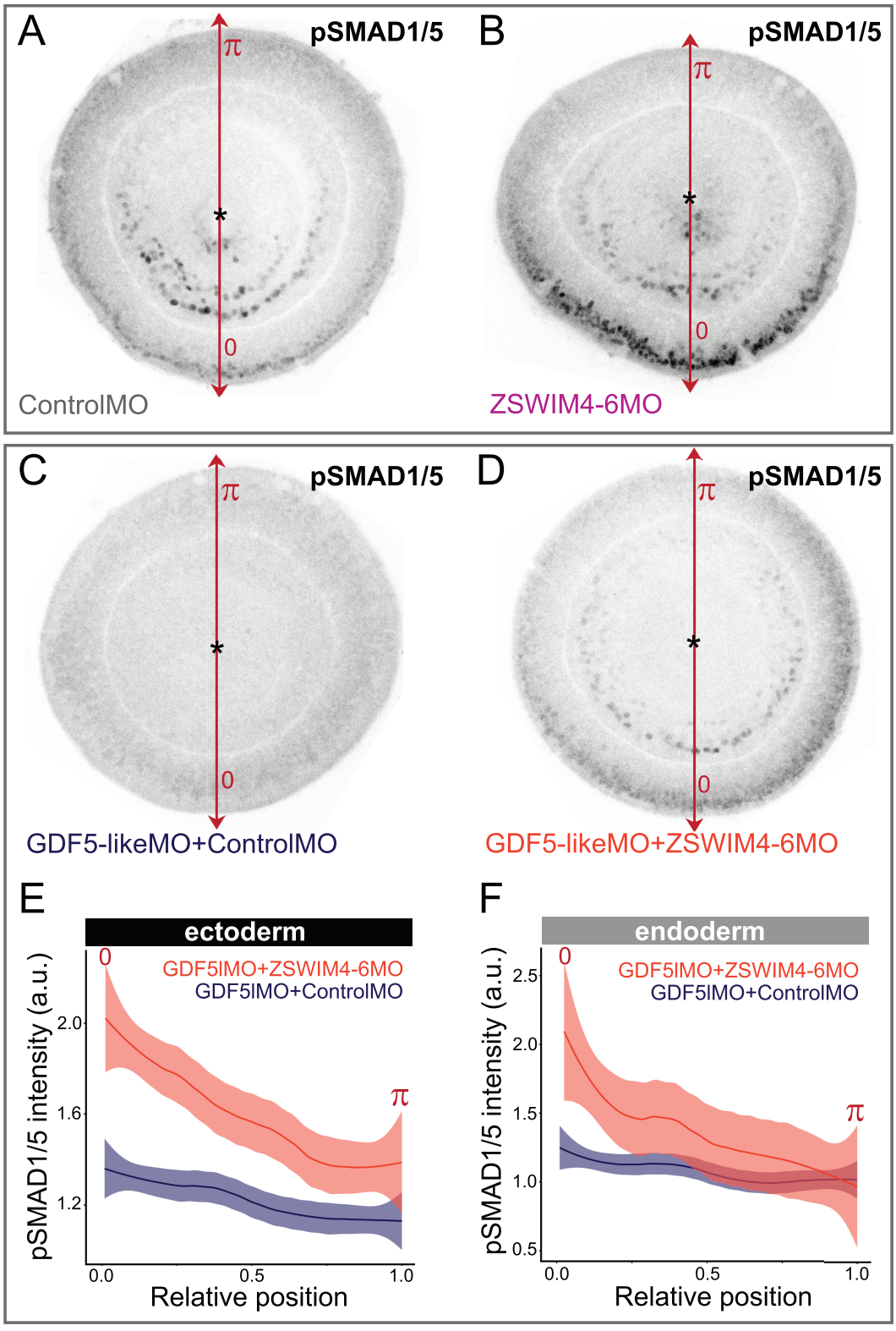

Figure 6—figure supplement 3. ZSWIM4-6 knockdown partially rescues the reduction of pSMAD1/5 caused by GDF5-like knockdown. Oral views of 2 dpf embryos stained for pSMAD1/5. (**A, B**) Embryos injected with control morpholino and ZSWIM4-6MO show phenotypes identical to the ones presented in ***Figure 6C and C'***. (**C, D**) Embryos injected with GDF5lMO together with either Control MO (**C**) or ZSWIM4-6MO (**D**). pSMAD1/5 is strongly reduced upon GDF5lMO injection (**C**), but partially rescued by co-injection of ZSWIM4-6MO (**D**). (**E, F**) Quantification of the ectodermal (**E**) and the

Figure 6—figure supplement 3 continued on next page

Figure 6—figure supplement 3 continued

endoderm (**F**) nuclear pSMAD1/5 staining intensity in the GDF5IMO morphants. Nuclear staining intensity (arbitrary units, a.u.) is plotted as a function of the relative position of each nucleus in the endoderm or in the ectoderm along a 180° arc from 0 (high signaling side) to π (low signaling side). The measurements from GDF5IMO + ControlMO embryos (n = 9) and GDF5IMO + ZSWIM4-6MO embryos (n = 16) are described by a LOESS smoothed curve (solid line) with a 99% confidence interval for the mean (shade).

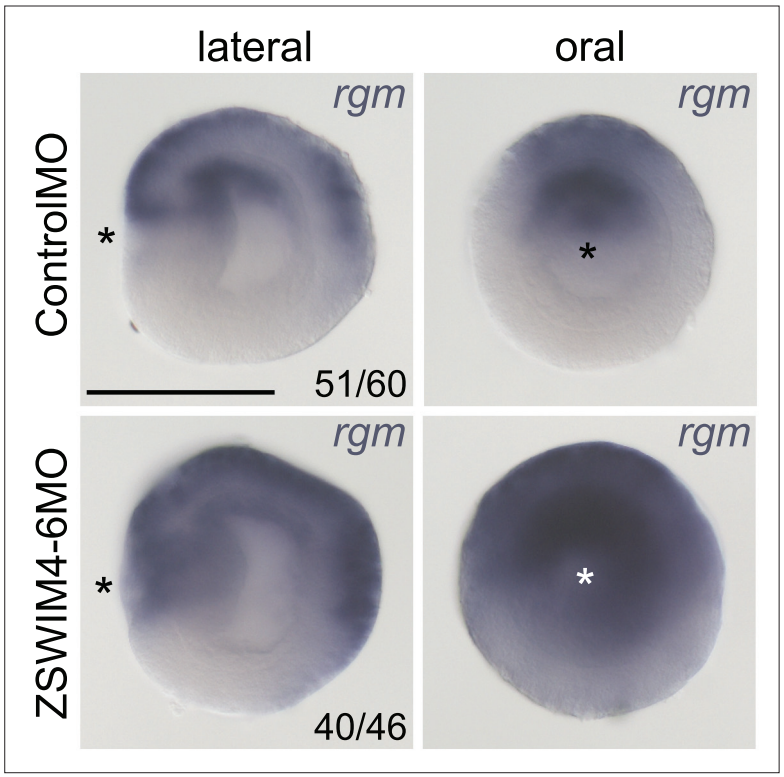

Figure 6—figure supplement 4. *rgm* expression expands upon ZSWIM4-6 knockdown. In situ hybridization on 2d planulae. Asterisks denote the location of the blastopore. Scale bar 100 µm.

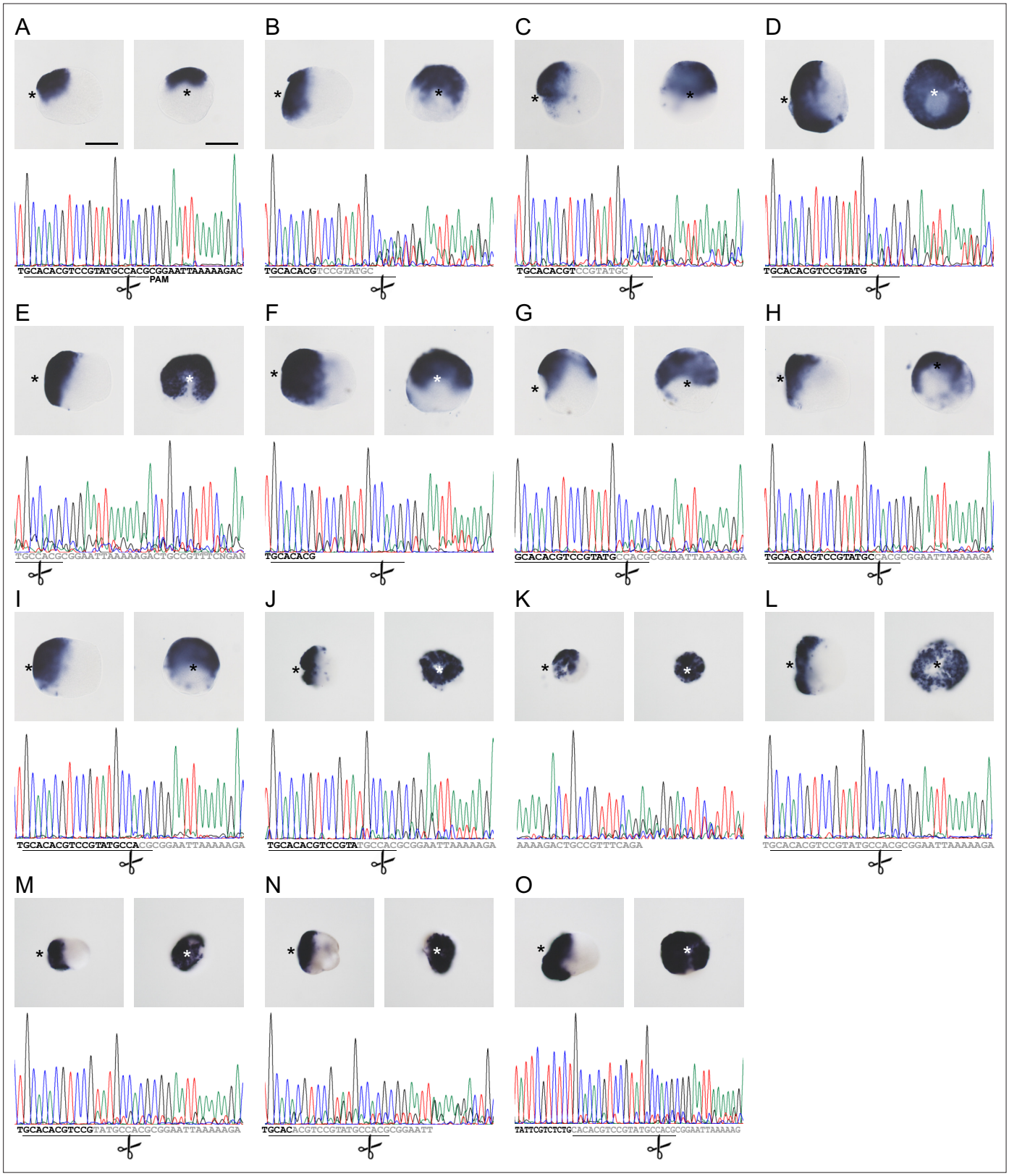

Figure 6—figure supplement 5. CRISPR/Cas9-mediated mutagenesis of *zswim4-6* results in the expansion of *chordin* expression in mosaic mutants (F0). (**A**) Bilateral expression of *chordin* in wild-type 2d planula and corresponding sequencing chromatogram of *zswim4-6_g254* target region. (**B–O**) Expanded or radialized chordin expression in 2d mutant planulae injected with a single guide RNA (**B–I**) or two guide RNAs (**J–O**) targeting the SWIM zinc-finger domain. Corresponding sequencing chromatograms show sequence variability (overlapping peaks, gray or no letters) in the vicinity of the

Figure 6—figure supplement 5 continued on next page

Figure 6—figure supplement 5 continued

targeting locus of the *zswim4-6_g254* gRNA in individual mutant embryos. The protospacer sequence is underlined, the position of the PAM is shown on (**A**). Scissors indicate the Cas9 cutting site. In the in situ hybridization images, asterisks mark the oral side, scale bars 100 µm.